Chemical Physics Letters 800 (2022) 139673

Contents lists available at ScienceDirect

Chemical Physics Letters

journal homepage: www.elsevier.com/locate/cplett

The light detection performance of the congo red dye in a Schottky type photodiode

Adem Kocyigit [a,*], Mehmet Yılmaz [b,c,**], Ümit İncekara [d,e], Yılmaz Şahin [f], Şakir Aydoğan [f]

[a] Department of Electronics and Automation, Vocational High School, Bilecik Şeyh Edebali University, 11230 Bilecik, Turkey
[b] Advanced Materials Research Laboratory, Department of Nanoscience and Nanoengineering, Graduate School of Natural and Applied Sciences, Ataturk University, 25240 Erzurum, Turkey
[c] Department of Science Teaching, Faculty of K.K. Education, Ataturk University, 25240 Erzurum, Turkey
[d] Department of Molecular Biology and Genetics, Faculty of Science, Erzurum Technical University, Erzurum, Turkey
[e] Department of Biology, Faculty of Science, Atatürk University, 25240 Erzurum, Turkey
[f] Department of Physics, Faculty of Sciences, Atatürk University, 25240 Erzurum, Turkey

ARTICLE INFO

Keywords:
Congo red
Metal-semiconductor devices
Photodiodes
Responsivity

ABSTRACT

The Congo red (CR) (3,3′-[(1,1′,-biphenyl)-4,4′-diyl)bis(4-amino-1 amino naphthalene sulphonic)]) is usually used for staining of amyloidosis diseases in the diagnostic application. It shows dichroic behavior, and thus can be employed in optoelectronic applications. In this study, commercially purchased congo red dye was used as an interfacial organic layer for Schottky type photodiode to understand its sensitivity to light. The surface morphology of the CR interlayer was investigated by scanning electron microscopy (SEM), and almost uniform surface was obtained. While cobalt (Co) element was employed as metallic contact, the *n*-type Si and aluminum (Al) were used as a semiconductor and ohmic contact, respectively. Thus, Co/CR/*n*-Si device was fabricated by a spin coating and thermal evaporation technique, and characterized by *I-V* measurements under dark and various light power intensities. The results revealed that the congo red dye can be improved and employed for optoelectronic applications.

1. Introduction

The compatibility to the environment, flexibility, healthy and low-cost behaviors make organic materials interesting for various areas and researchers [1-3]. They can be used in light-emitting diodes (LEDs), photodetectors, photodiodes, solar cells, and field-effect transistors (FETs) [4-8]. There are many organic materials such as Eosin Y, Tris(8-hydroxyquinoline) aluminum, rubrene, pentacene, tetracene, congo red and Poly(3-hexylthiophene-2,5-diyl), perylene-diimide and coronene which they have been used in various applications for organic devices [9-13]. Among them, congo red is a kind of dye with $C_{32}H_{22}N_6Na_2O_6S_2$ chemical formula and can be employed for optoelectronic applications [14].

Photodiodes are used for the detection of light at reverse biases because the depletion region width of the junction increased and remained only light-induced charges. Thus, light-induced charges cause at the current, and so the light is detected by photodiodes [15]. Generally, PIN diodes are used and preferred for photodiode application, but they have a long reaction time due to having both *n*- and *p*-diffusion tail regions. Another type of photodiode is Schottky type photodiode, and it has a shorter response time. Various organic materials can be employed for increasing the efficiency of Schottky-type photodiodes. For example, Srivastava *et al.* fabricated Al/pentacene/ITO heterostructure photodiode for ultraviolet detection, and the photodiode exhibited high sensitivity and detectivity [16]. Kumar *et al.* studied photodiode behavior of the Au/CdSe QDs/ZnO QDs/*n*-Si heterostructure which CdSe was used as an active layer and ZnO QDs was employed as a transport layer, and the results revealed that the fabricated photodiode exhibited high responsivity and low barrier height [17]. Cifci *et al.* fabricated Al/perovskite/*p*-Si heterojunction by using $CH_3NH_3PbI_{3-x}Cl_x$ perovskite material for photodiode applications. They concluded that the perovskite layer caused to increase the photocurrent

* Corresponding author.
** Corresponding author at: Advanced Materials Research Laboratory, Department of Nanoscience and Nanoengineering, Graduate School of Natural and Applied Sciences, Ataturk University, 25240 Erzurum, Turkey.
E-mail addresses: adem.kocyigit@bilecik.edu.tr (A. Kocyigit), mehmetyilmaz@atauni.edu.tr (M. Yılmaz).

https://doi.org/10.1016/j.cplett.2022.139673
Received 18 January 2022; Received in revised form 15 March 2022; Accepted 29 April 2022
Available online 5 May 2022

of the photodiode, enormously [18]. There are many studies to use organic materials in the interface of the Schottky type photodiodes in the literature due to advantage of them for flexibility, wearability etc. [19,20].

In this study, we employed the congo red dye as an interfacial layer between the Co metal and *n*-Si semiconductor to test the efficiency of the Co/CR/*n*-Si photodiode due to successful application of congo red in light-induced photoisomerization and reversible optical data storage. Diode and photodiode properties of the Co/CR/*n*-Si heterostructure were investigated by *I-V* measurements under dark and various light power intensities.

2. Experimental details

Commercially purchased congo red dye from Sigma Aldrich were employed without purification for Schottky type photodiode device. Firstly, 0.5 g congo red dye was filled in a vessel and dissolved in water by stirring for one hour to obtain 0.2 M solution. Secondly, a whole (1 0 0) oriented *n*-Si wafer with 1–10 Ω.cm resistivity, 7.5×10^{16} cm^{-3} carrier concentration and 400 μm thicknesses was sliced into 1.5 cm^2 pieces, and then the pieces were cleaned by acetone, deionized water and isopropanol in an ultrasonic cleaner. Thirdly, aluminum metal was evaporated on the back surfaces of the *n*-Si wafer pieces by thermal evaporation technique, and they were immediately transferred into N_2 filled oven to form ohmic contact for four minutes. Fourthly, the congo red solution was coated on front surfaces of *n*-Si pieces by spin coating technique at 3000 rpm in 30 s. Finally, the congo red film surfaces were deposited with cobalt metal by thermal evaporator using a 7.85×10^{-3} cm^2 holed array mask. The fabricated Co/CR/*n*-Si photodiodes and schematic light illumination diamgrams have been displayed in Fig. 1. Keithley 2400 *I-V* source meter was performed on the Co/CR/*n*-Si photodiodes with Sciencetech solar simulator (AM1.5 G or solar spectrum) to obtain *I-V* measurements under dark and various light power intensities in the range of 100 mW/cm^2 and 400 mW/cm^2. The morphology of the CR was obtained by FEI/Quanta 450 FEG SEM.

3. Results and discussion

SEM image of the CR interlayer have been indicated in Fig. 2 for 10000x magnification. The surface of the CR layer is free from pinhole or defects. However, the surface exhibited some of roughness due to organic behavior of the CR interlayer. Even if existing of some rough parts, the surface of the CR layer is almost uniform, and it can be used efficiently for photodiode applications as interlayer.

Reverse bias *I-V* characteristics of the Co/CR/*n*-Si photodiode have been shown in Fig. 3 for increasing light power intensity from 100 mW/cm^2 to 400 mW/cm^2. The reverse bias current was obtained as around

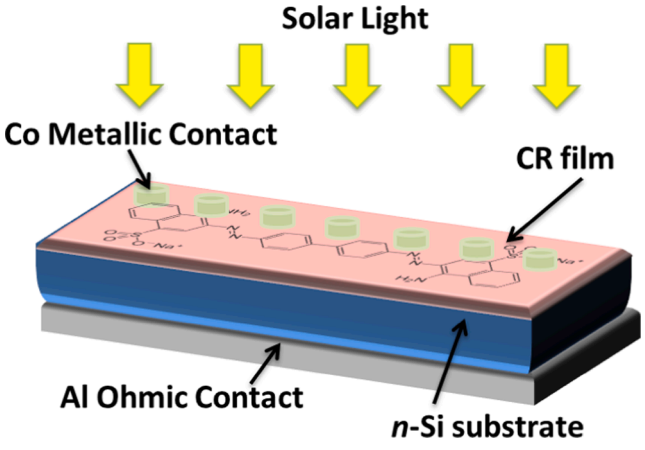

Fig. 1. The diagrammatic exhibition of the fabricated Co/CR/*n*-Si photodiodes.

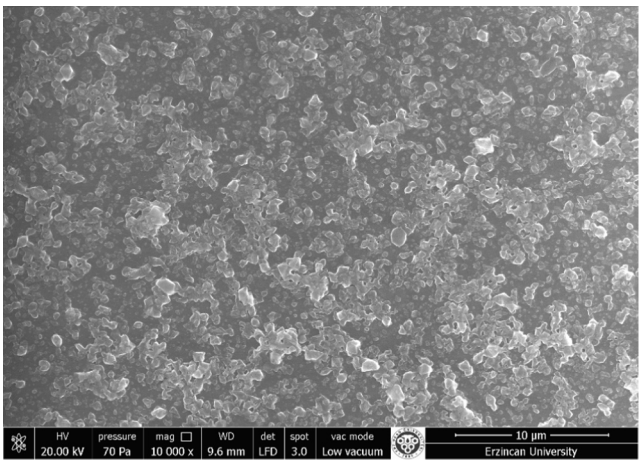

Fig. 2. SEM image of the CR interlayer.

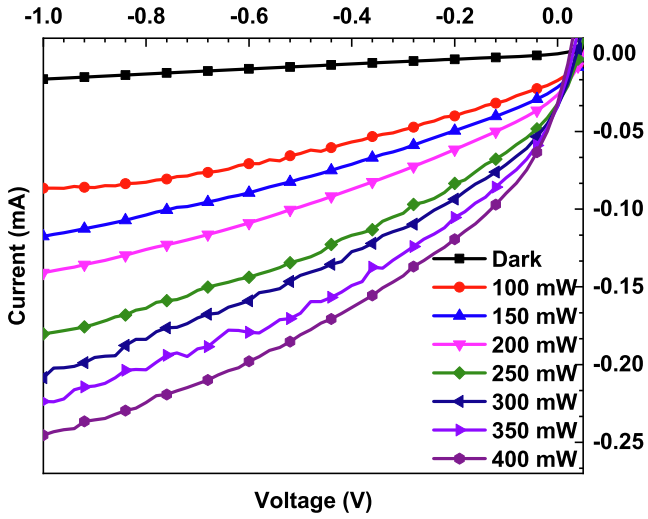

Fig. 3. Reverse bias *I-V* characteristics of the Co/CR/*n*-Si photodiodes for various light power intensities.

10–16 μA for dark and increased clearly with increasing light power up to 86 μA at −1 V for 100 mW/cm^2 due to increasing light-induced charges. Furthermore, the photocurrent values increased almost linearly for every light power intensity after then 100 mW/cm^2. The results confirmed the photodiode behavior of the Co/CR/*n*-Si heterojunctions [21]. The physical mechanism behind the Co/CR/*n*-Si photodiode can be attributed to the increasing of charge carriers in the interface by light illumination at reverse biases. The Co/CR/*n*-Si photodiode had a wide depletion region at the reverse bias, and thus the light caused to increase the amounts of mobile charges or photocurrent. Therefore, the light can be detected by the Co/CR/*n*-Si photodiode. The CR layer also can capture photons and emits electrons at reverse biases and contribute to the photocurrent of the Co/CR/*n*-Si photodiode.

Semi logarithmic *I-V* characteristics of the Co/CR/*n*-Si photodiode for reverse and forward biases have been displayed in Fig. 4. Both the reverse and forward bias currents have exhibited increment with increasing light power intensity due to having sensitivity behavior of the Co/CR/*n*-Si heterostructure for detection of light. The light caused to increase of more mobility charge at forwarding biases, and thus the current increased by an increment of the light power. Moreover, the shifting behavior of the current with increasing light power at forward biases can be ascribed to the photovoltaic behavior of the Co/CR/*n*-Si [22]. The inset of Fig. 4 and Table 1 exhibit rectifying ratio (*RR*) changes of the Co/CR/*n*-Si photodiode depending on the changing light power

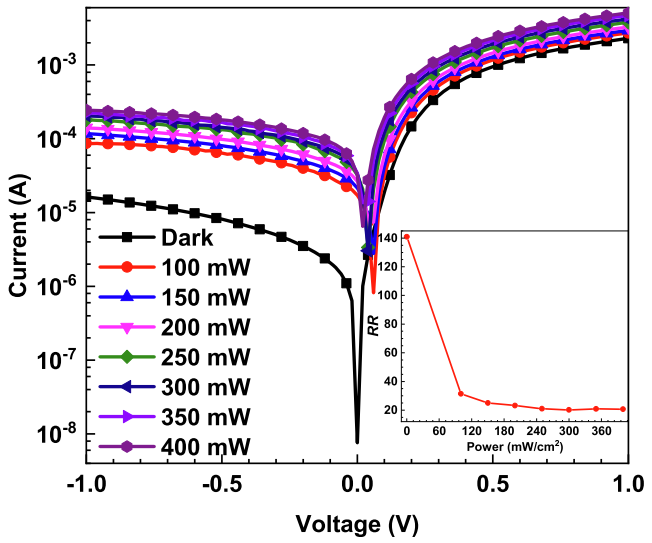

Fig. 4. Semi-logarithmic *I-V* characteristics of the Co/CR/*n*-Si photodiodes for various light power intensities.

intensity for ±1 V. The increasing light power caused to decrease at the rectifying ratio due to increasing photocurrent at reverse biases more than forwarding biases. Although the rectifying ratio values decreased with increasing light power, the Co/CR/*n*-Si photodiode exhibited still rectifying behavior, and the rectifying ratio values indicated a stable profile towards higher light power intensities.

I-V characteristics can be used to calculate ideality factor (n), barrier height ($\varnothing_b$) and resistance (shunt and series) values of a diode. Thermionic emission theory can be performed to calculate the n and $\varnothing_b$ values of the Co/CR/*n*-Si photodiode. The changes at the calculated n and $\varnothing_b$ values of the Co/CR/*n*-Si photodiode by various light power intensities have been given in Fig. 5, and their values have been listed in Table 1. While the barrier height values usually decreased from 0.66 eV to 0.56 eV, ideality factor values increased from 1.07 to 2.28 with increasing light power intensity for the Co/CR/*n*-Si photodiode. Both the ideality factor and barrier height values are in good agreement with literature for a kind of Schottky-type photodiode. The ideality factor value of the Co/CR/*n*-Si photodiode is close to unity and confirms the good diode behavior. The small deviation from linearity can be attributed to barrier inhomogeneity in the interface of the photodiode [23].

The series and shunt resistances are critical parameters to obtain a good photodiode for optoelectronic applications and determined from the junction resistance [24]. While the reverse bias region of the junction resistance shows shunt resistance (R_{sh}), the forward bias region of the junction resistance after knee voltage value displays series resistance (R_s) [25]. Fig. 6 indicates the junction resistance profile of the Co/CR/*n*-Si changing light power intensities. While the R_s values decreased from 350 Ω to 170 Ω with increasing light power intensity, the R_{sh} values decreased from 65 kΩ to 15 kΩ. The decrement at the resistance values can be based on the increasing charge carrier with increasing light power. The determined series and shunt resistance values implied well device characteristics [26]. There are other techniques to calculate series resistance according to literature such as classical Norde, Cheung and new technique Ocaya-Yakuphanoğlu [27-30].

Another method to check or confirm the barrier height and to determine series resistance is the Norde method [27]. The Norde method is established on the Norde function ($F(v)$), and this function changes depending on the voltage. By plotting of this function against to voltage, the barrier height and series resistance are obtained by minimum $F(v)$

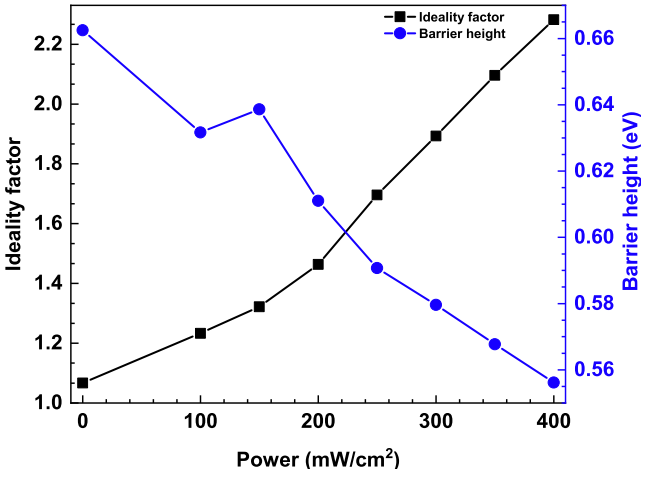

Fig. 5. The ideality factor and barrier height changes of the Co/CR/*n*-Si for increasing light power intensity S.

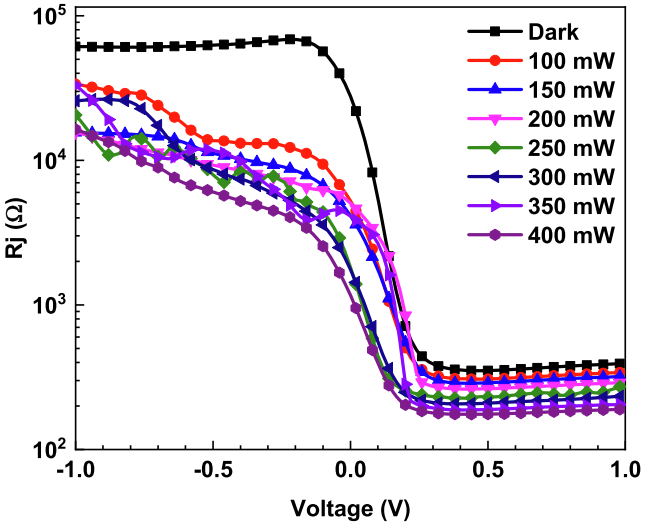

Fig. 6. R_j-V plots of the Co/CR/*n*-Si photodiodes for various light illumination power intensities.

Table 1
Various heterostructure parameters of the Co/CR/*n*-Si photodiode.

Power (mW/cm²)	Saturation Current (I_0) (A)	n (*I-V*) (-)	$\varnothing_b$ (*I-V*) (eV)	Built-in Voltage (V)	Responsivity (mA/W)	Detectivity (D* Jones)	*RR* (-)
Dark	6.01×10^{-7}	1.07	0.66	0.16	–	–	140.93
100	1.98×10^{-6}	1.23	0.63	0.13	21.87	3.93×10^{10}	31.43
150	2.65×10^{-6}	1.32	0.62	0.12	18.29	3.28×10^{10}	25.03
200	4.39×10^{-6}	1.46	0.61	0.11	16.83	3.02×10^{10}	23.20
250	9.63×10^{-6}	1.70	0.59	0.10	16.44	2.95×10^{10}	20.97
300	1.48×10^{-5}	1.89	0.58	0.09	14.36	2.58×10^{10}	20.15
350	2.34×10^{-5}	2.10	0.57	0.09	12..32	2.21×10^{10}	20.92
400	3.66×10^{-5}	2.28	0.56	0.08	10.14	1.82×10^{10}	20.70

and related voltage value. Fig. 7 exhibits Norde function versus voltage plots of the Co/CR/*n*-Si photodiode for dark. While the barrier height was obtained as 0.67 eV, the series resistance was calculated as 313 Ω. The determined barrier height value is in good harmony with the thermionic emission barrier height. The calculated series resistance value is also in good agreement with obtained junction resistance plot for dark.

Cheung method also can be employed to confirm the accuracy of the diode parameters which are obtained by thermionic emission and Norde methods [28]. Cheung method asserted $dV/d(\ln I)$ and $H(I)$ functions, and they change linearly by the forward bias current. Thus, the ideality and barrier height values are obtained by the *y*-intercept values of the $dV/d(\ln I)$ and $H(I)$ functions, respectively [31]. The slopes of the two functions provide to determine two different series resistances which are close to each other [24]. Fig. 8 shows the $dV/d(\ln I)$ and $H(I)$ functions against to current for the Co/CR/*n*-Si photodiode under dark condition. Both functions exhibited good linearity for a wide range of current changes and helped to calculate the diode parameters. While the ideality factor was calculated as 1.16, the barrier height was obtained as 0.65 eV. The series resistance values were determined as 322 Ω for $dV/d(\ln I)$ plot and 312 Ω for $H(I)$ plot. The determined diode parameters for the Co/CR/*n*-Si photodiode from the Cheung method exhibited good agreement with other techniques [32].

The input–output gain of the photodiode can be studied by plotting the responsivity (R) depending on the voltage changes [33]. The responsivity values are calculated by:

$$R = \frac{I_p}{PA} \tag{1}$$

where I_p is photocurrent and calculated by the difference between the light current and dark current, P and A show the light power and diode area, respectively. The responsivity versus voltage plots of the Co/CR/*n*-Si photodiode has been indicated in Fig. 9 for increasing light power intensity. The photodiode exhibited high responsivity values, but their values usually decreased with increasing light power and decrease reverse bias. The reason for the decreasing with increasing light power can be attributed to the reciprocal relation between light power and responsivity.

The profile of the photocurrent and photosensitivity with increasing light power is important to understand the conduction mechanism of a photodiode. The relation between the photocurrent and light power is given by $I_{ph} = AP^m$ where A and m are photocurrent constant and exponent values, respectively. The m can be determined from the slope of logarithmic photocurrent versus power graph [34]. If m is bigger than

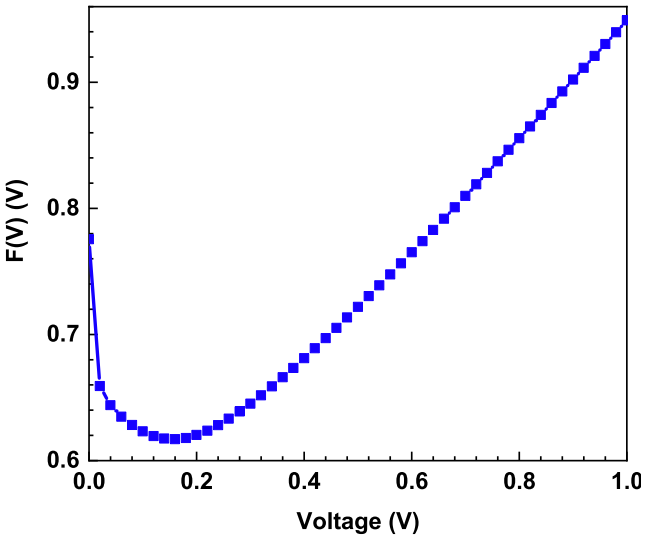

Fig. 7. *F(v)-V* characteristics of the Co/CR/*n*-Si photodiode.

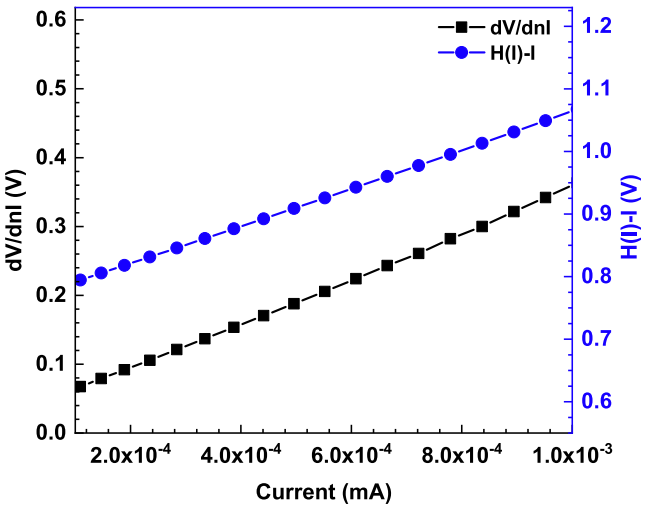

Fig. 8. Cheung plots of the Co/CR/*n*-Si photodiode.

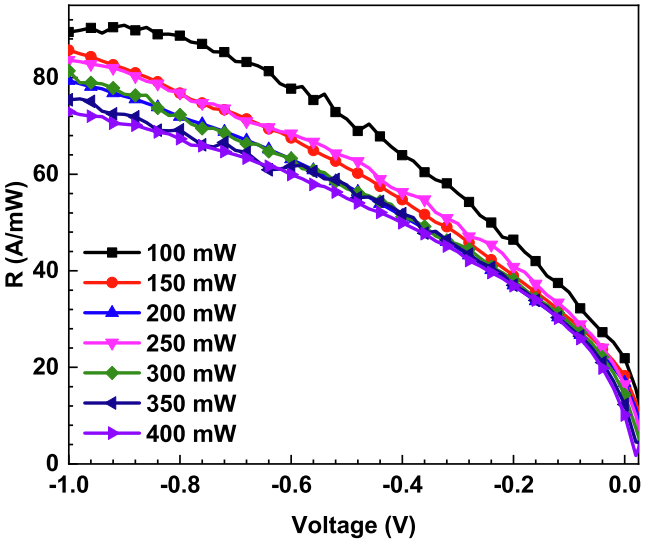

Fig. 9. Responsivity versus voltage plots of the Co/CR/*n*-Si photodiode.

one, the photoconductivity mechanism is dominant. If the m value changes in between 0.5 and 1.0, the trap levels distribution control the conduction mechanism cautiously. Fig. 10a indicates the photocurrent and photosensitivity profile of the Co/CR/*n*-Si photodiode depending on the light power intensity. Both the current and photosensitivity values increased up to 250 mW/cm^2 light power almost linearly and then slightly decreased for 400 mW/cm^2 light power. This kind of profile can be attributed to the photoconduction mechanism from 100 mW/cm^2 to 250 mW/cm^2 light power and continuous distribution evanescent trap levels from 250 mW/cm^2 to 400 mW/cm^2 for the Co/CR/*n*-Si photodiode. The high light power intensity may be caused to increase trap levels due to increasing degradation of the congo red layer [35].

The specific detectivity (D^*) is another detection parameter and calculated by the below formula depending on the responsivity:

$$D^* = R\sqrt{\frac{A}{2qI_{dark}}} \tag{2}$$

where q is the charge of the electron.

Fig. 10b indicates light intensity dependent profile of the responsivity and specific detectivity values. Their values have been also listed in Table 1 at 0 voltage value for increasing light power intensity. Both

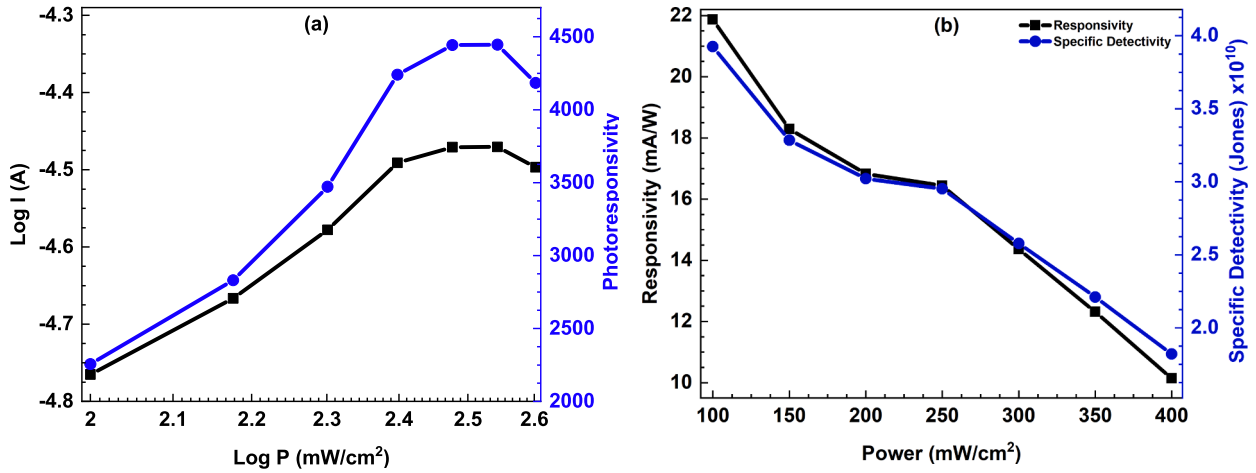

Fig. 10. (**a**) Photocurrent and photoresponsivity, (**b**) responsivity and specific detectivity changes of the Co/CR/*n*-Si photodiode depending on the light power intensity.

the responsivity and specific detectivity values decreased with increasing light power. The obtained values are good agreement with literature, and the Co/CR/*n*-Si photodiode can be used photodetection applications [36-38].

4. Conclusion

The congo red film was synthesized onto the *n*-Si by spin coating technique and employed as an interfacial layer between the Co metal and *n*-Si. The SEM image of the CR surface revealed almost uniform and pinhole free structures. The fabricated Co/CR/*n*-Si photodiode was characterized by *I-V* measurements under dark and various light power intensities. The Co/CR/*n*-Si heterostructure exhibited photodiode behavior by giving the response light power intensity changes. Various diode parameters such as series resistance, shunt resistance, barrier height, and ideality factor as well as detection parameters of responsivity and detectivity values were calculated and discussed in detail for the Co/CR/*n*-Si photodiode. The obtained results revealed that the congo red-based photodiodes can be improved for optoelectronic applications.

CRediT authorship contribution statement

Adem Kocyigit: Writing – review & editing. **Mehmet Yılmaz:** Visualization, Investigation. **Ümit İncekara:** Conceptualization, Methodology. **Yılmaz Şahin:** Data curation. **Şakir Aydoğan:** Supervision.

Declaration of Competing Interest

The authors declare that they have no known competing financial interests or personal relationships that could have appeared to influence the work reported in this paper.

Acknowledgements

Authors would like to thank H. Kacus for her helps.

References

[1] P.C.Y. Chow, T. Someya, Organic Photodetectors for Next-Generation Wearable Electronics, Adv. Mater. 32 (15) (2020) 1902045, https://doi.org/10.1002/adma.201902045.
[2] H. Ling, S. Liu, Z. Zheng, F. Yan, Organic Flexible Electronics, Small Methods. 2 (10) (2018) 1800070, https://doi.org/10.1002/smtd.201800070.
[3] J.S. Chang, A.F. Facchetti, R. Reuss, A Circuits and Systems Perspective of Organic/Printed Electronics: Review, Challenges, and Contemporary and Emerging Design Approaches, IEEE J. Emerg. Sel. Top. Circuits Syst. 7 (1) (2017) 7–26, https://doi.org/10.1109/JETCAS.2017.2673863.
[4] H. Cho, C.-W. Byun, C.-M. Kang, J.-W. Shin, B.-H. Kwon, S. Choi, N.S. Cho, J.-I. Lee, H. Kim, J.H. Lee, M. Kim, H. Lee, White organic light-emitting diode (OLED) microdisplay with a tandem structure, J. Inf. Disp. 20 (4) (2019) 249–255, https://doi.org/10.1080/15980316.2019.1671240.
[5] Y. Wang, J. Zhang, S. Zhang, J. Huang, OFET chemical sensors: Chemical sensors based on ultrathin organic field-effect transistors, Polym. Int. 70 (4) (2021) 414–425, https://doi.org/10.1002/pi.6095.
[6] F. Kabir, S.N. Sakib, N. Matin, Stability study of natural green dye based DSSC, Optik (Stuttg). 181 (2019) 458–464, https://doi.org/10.1016/j.ijleo.2018.12.077.
[7] L. Shi, Q. Liang, W. Wang, Y. Zhang, G. Li, T. Ji, Y. Hao, Y. Cui, Research progress in organic photomultiplication photodetectors, Nanomaterials. 8 (2018) 713, https://doi.org/10.3390/nano8090713.
[8] G.-H. Nam, K. Kim, D.S. Chung, Non-power-driven organic photodiode via junction engineering, Nanotechnology. 30 (5) (2019) 055202, https://doi.org/10.1088/1361-6528/aaf030.
[9] A. Karabulut, İ. Orak, S. Canlı, N. Yıldırım, A. Türüt, Temperature-dependent electrical characteristics of Alq3/p-Si heterojunction, Phys. B Condens. Matter. 550 (2018) 68–74, https://doi.org/10.1016/j.physb.2018.08.029.
[10] H. Kacus, M. Yilmaz, A. Kocyigit, U. Incekara, S. Aydogan, Optoelectronic properties of Co/pentacene/Si MIS heterojunction photodiode, Phys. B Condens. Matter. 597 (2020) 412408.
[11] Ö.F. Yüksel, N. Tuğluoğlu, F. Çalışkan, M. Yıldırım, Temperature Dependence of Current-Voltage Characteristics of Al/Rubrene/n-GaAs (100) Schottky Barrier Diodes, Mater. Today Proc., Elsevier 3 (5) (2016) 1271–1276, https://doi.org/10.1016/j.matpr.2016.03.070.
[12] Ü. Akın, Ö.F. Yüksel, N. Tuğluoğlu, Dielectric Properties of Coronene Film Deposited onto Silicon Substrate by Spin Coating for Optoelectronic Applications, Silicon. 14 (5) (2022) 2201–2209, https://doi.org/10.1007/s12633-021-01017-3.
[13] Ö.F. Yüksel, M. Kuş, M. Yıldırım, Capacitance and Conductance-Frequency Characteristics of Au/n-Si Schottky Structure with Perylene-Diimide (PDI) Organic Interlayer, J. Electron. Mater. 46 (2) (2017) 882–887, https://doi.org/10.1007/s11664-016-4999-y.
[14] A. Kocyigit, M. Yilmaz, S. Aydogan, Ü. İncekara, H. Kacus, Comparison of n and p type Si-based Schottky photodiode with interlayered Congo red dye, Mater. Sci. Semicond. Process. 135 (2021) 106045, https://doi.org/10.1016/j.mssp.2021.106045.
[15] Y. Wei, T. Lehmann, L. Silvestri, H. Wang, F. Ladouceur, Photodiode working in zero-mode: detecting light power change with DC rejection and AC amplification, Opt. Express. 29 (12) (2021) 18915.
[16] A. Srivastava, S. Jit, S. Tripathi, High-Performance Solution-Processed Pentacene/Al Schottky Ultraviolet Photodiode with Pseudo Photovoltaic Effect, IEEE Trans. Electron Devices. 67 (10) (2020) 4300–4307, https://doi.org/10.1109/TED.2020.3013557.
[17] H. Kumar, Y. Kumar, B. Mukherjee, G. Rawat, C. Kumar, B.N. Pal, S. Jit, Electrical and Optical Characteristics of Self-Powered Colloidal CdSe Quantum Dot-Based Photodiode, IEEE J. Quantum Electron. 53 (3) (2017) 1–8, https://doi.org/10.1109/JQE.2017.2696487.
[18] O.S. Cifci, A. Kocyigit, P. Sun, Perovskite/p-Si photodiode with ultra-thin metal cathode, Superlattices Microstruct. 120 (2018) 492–500, https://doi.org/10.1016/J.SPMI.2018.06.009.
[19] Ö.F. Yüksel, N. Tuğluoğlu, H. Şafak, M. Kuş, The modification of Schottky barrier height of Au/p-Si Schottky devices by perylene-diimide, J. Appl. Phys. 113 (4) (2013) 044507, https://doi.org/10.1063/1.4789021.
[20] N. Tuğluoğlu, F. Çalişkan, F. Yüksel, Analysis of inhomogeneous barrier and capacitance parameters for Al/rubrene/n-GaAs (100) Schottky diodes, Synth. Met. 199 (2015) 270–275, https://doi.org/10.1016/j.synthmet.2014.10.027.

[21] B. Ezhilmaran, A. Patra, S. Benny, S. M. r., A. V. v., S.V. Bhat, C.S. Rout, Recent developments in the photodetector applications of Schottky diodes based on 2D materials, J. Mater. Chem. C. 9 (19) (2021) 6122–6150.
[22] B. Tatar, A.E. Bulgurcuoğlu, P. Gökdemir, P. Aydoğan, D. Yılmazer, O. Özdemir, K. Kutlu, Electrical and photovoltaic properties of Cr/Si Schottky diodes, Int. J. Hydrogen Energy. 34 (12) (2009) 5208–5212, https://doi.org/10.1016/j.ijhydene.2008.10.040.
[23] M. Özer, D.E. Yıldız, Ş. Altındal, M.M. Bülbül, Temperature dependence of characteristic parameters of the Au/SnO2/n-Si (MIS) Schottky diodes, Solid. State. Electron. 51 (6) (2007) 941–949, https://doi.org/10.1016/j.sse.2007.04.013.
[24] A. Kocyigit, M. Yıldırım, A. Sarılmaz, F. Ozel, The Au/Cu2WSe4/p-Si photodiode: Electrical and morphological characterization, J. Alloys Compd. 780 (2019) 186–192, https://doi.org/10.1016/j.jallcom.2018.11.372.
[25] L.D. Rao, V.R. Reddy, Electrical parameters and series resistance analysis of Au/Y/p-InP/Pt Schottky barrier diode at room temperature, in: AIP Conf. Proc., AIP Publishing LLC, 2016: p. 120020. https://doi.org/10.1063/1.4948092.
[26] İ. Taşçıoğlu, W.A. Farooq, R. Turan, Ş. Altındal, F. Yakuphanoglu, Charge transport mechanisms and density of interface traps in MnZnO/p-Si diodes, J. Alloys Compd. 590 (2014) 157–161, https://doi.org/10.1016/J.JALLCOM.2013.12.043.
[27] H. Norde, A modified forward I-V plot for Schottky diodes with high series resistance, J. Appl. Phys. 50 (7) (1979) 5052–5053, https://doi.org/10.1063/1.325607.
[28] S.K. Cheung, N.W. Cheung, Extraction of Schottky diode parameters from forward current-voltage characteristics, Appl. Phys. Lett. 49 (2) (1986) 85–87, https://doi.org/10.1063/1.97359.
[29] I. Taşçioğlu, W.A. Farooq, R. Turan, Ş. Altindal, F. Yakuphanoglu, Charge transport mechanisms and density of interface traps in MnZnO/p-Si diodes, J. Alloys Compd. 590 (2014) 157–161, https://doi.org/10.1016/j.jallcom.2013.12.043.
[30] R.O. Ocaya, F. Yakuphanoğlu, Ocaya-Yakuphanoğlu method for series resistance extraction and compensation of Schottky diode I-V characteristics, Meas. J. Int. Meas. Confed. 186 (2021) 110105, https://doi.org/10.1016/j.measurement.2021.110105.
[31] I. Orak, A. Kocyigit, A. Turut, The surface morphology properties and respond illumination impact of ZnO/n-Si photodiode by prepared atomic layer deposition technique, J. Alloys Compd. 691 (2017) 873–879, https://doi.org/10.1016/j.jallcom.2016.08.295.
[32] H.H. Gullu, D.E. Yildiz, A. Kocyigit, M. Yıldırım, Electrical properties of Al/PCBM: ZnO/p-Si heterojunction for photodiode application, J. Alloys Compd. 827 (2020) 154279, https://doi.org/10.1016/j.jallcom.2020.154279.
[33] G. Luongo, F. Giubileo, L. Genovese, L. Iemmo, N. Martucciello, A. Di Bartolomeo, I-V and C-V characterization of a high-responsivity graphene/silicon photodiode with embedded MOS capacitor, Nanomaterials. 7 (2017) 158, https://doi.org/10.3390/nano7070158.
[34] N.M. Khusayfan, Electrical and photoresponse properties of Al/graphene oxide doped NiO nanocomposite/p-Si/Al photodiodes, J. Alloys Compd. 666 (2016) 501–506, https://doi.org/10.1016/j.jallcom.2016.01.102.
[35] E. Laureto, M.A.T. da Silva, R.V. Fernandes, J.L. Duarte, I.F.L. Dias, H. de Santana, A. Marletta, Laser irradiation effects on the optical properties of layer-by-layer PPV/Congo Red thin films, Synth. Met. 161 (1-2) (2011) 87–91, https://doi.org/10.1016/j.synthmet.2010.11.002.
[36] L. Zeng, L. Tao, C. Tang, B.o. Zhou, H. Long, Y. Chai, S.P. Lau, Y.H. Tsang, High-responsivity UV-Vis Photodetector Based on Transferable WS2 Film Deposited by Magnetron Sputtering, Sci. Rep. 6 (1) (2016), https://doi.org/10.1038/srep20343.
[37] M. Shkir, M.T. Khan, I.M. Ashraf, A. Almohammedi, E. Dieguez, S. AlFaify, High-performance visible light photodetectors based on inorganic CZT and InCZT single crystals, Sci. Rep. 9 (2019) 1–9, https://doi.org/10.1038/s41598-019-48621-3.
[38] C.H. Ji, K.T. Kim, S.Y. Oh, High-detectivity perovskite-based photodetector using a Zr-doped TiO: X cathode interlayer, RSC Adv. 8 (15) (2018) 8302–8309.